

Preparation and thermal properties of stearic acid/diatomite composites as form-stable phase change materials for thermal energy storage via direct impregnation method

Xiaowei Fu¹ · Zhimeng Liu¹ · Bo Wu¹ · Jiliang Wang² · Jingxin Lei¹

Received: 18 May 2015 / Accepted: 11 September 2015 / Published online: 21 September 2015
© Akadémiai Kiadó, Budapest, Hungary 2015

Abstract Stearic acid/diatomite composite form-stable phase change materials (PCMs) have been prepared by using a direct impregnation method without vacuum treatment. The surface morphology, chemical compatibility, thermal properties and thermal stability were characterized by scanning electron microscopy, Fourier transform infrared spectrometer and X-ray diffraction (XRD), differential scanning calorimeter and thermogravimetric analysis (TG), respectively. The results show that there are only physical interactions between stearic acid and diatomite in composite PCM. XRD analysis reveals that crystal type is not affected by composite technology of SA/diatomite composite form-stable PCM with decrease in crystal size due to the limited pores in diatomite. The melting and freezing temperatures of stearic acid/diatomite composite, respectively, are 52.3 and 48.4 °C. The latent heat of SA/diatomite composite reaches 57.1 J g⁻¹, potential to be used in a practical application. TG result indicates that the decomposition of SA/diatomite composite starts at 192 °C, implying that the SA/diatomite has a good thermal stability.

Keywords Composite phase change material · Thermal energy storage · Stearic acid · Thermal properties

Introduction

Latent heat energy storage based on phase change materials (PCMs) has attracted more and more attention for the ability to reduce energy consumption in the last two decades [1–3]. PCMs can absorb and release large amounts of heat during the phase transition process. For example, paving materials and heat transfer fluid containing PCMs will maintain near phase change temperature, resulting in thermal inertia [4–6]. For the widely used solid–fluid PCMs, the PCMs will change from solid state to fluid state once the external temperature is beyond their phase transition temperature (PTT) [7, 8]. Therefore, the encapsulation of solid–fluid PCMs should be carried out to prevent them from leaking out when melted.

Recently, more and more composite form-stable PCMs have been prepared by the encapsulation technology of microencapsulation and composite [9–11]. Sanchez et al. [12] reported that paraffin as low-temperature PCM was microencapsulated with polystyrene shell due to the high tensile strength and modulus. The 50 mass% of microcapsule was paraffin PCM. Song et al. [13] have studied the fabrication of the composite PCM microcapsules by the technique of in situ polymerization and with aminoplast as the wall and PCM bromo-hexadecane as the core. The silver nano-particles were distributed on the surface to increase wall toughness and strength. Meanwhile, silver as metallic filler is added to evidently enhance the thermal conductivity of PCM microcapsules, too. Xu et al. [14] revealed the preparation and thermal properties of paraffin/diatomite composite PCM using a direct impregnation method without vacuum treatment. The paraffin/diatomite composite form-stable PCM has melting temperature and latent heat of 41.11 °C and 70.51 J g⁻¹, respectively. Yang et al. [15] have prepared myristic–palmitic–stearic

✉ Jingxin Lei
jxlei@scu.edu.cn

Xiaowei Fu
xwfu@foxmail.com

¹ State Key Laboratory of Polymer Materials Engineering, Polymer Research Institute of Sichuan University, Chengdu 610065, China

² School of Chemistry Science and Engineering, Yunnan University, Kunming 650091, China

acid/expanded graphite composites as PCMs for thermal energy storage. The ternary fatty acid as PCM has the lower eutectic temperature (i.e., melting temperature), different from the phase change temperature of the corresponding single fatty acid. The melting temperature and latent heat were 42.99 °C and 153.5 J g⁻¹, respectively. Xu et al. [16] studied the system of paraffin/diatomite/multiwall carbon nanotubes composite PCMs, which was tailor-made for producing thermal energy storage cement-based composites. From the differential scanning calorimetry results, the form-stable composite PCM has melting temperature and latent heat of 27.12 °C and 89.40 J g⁻¹, respectively. Compared with microencapsulation using emulsion polymerization mentioned above, the direct impregnation method is an efficient and robust technology of encapsulation for various composite PCMs. Due to the capillary and surface tension [17], the organic PCMs absorbed into the porous or layered supporting materials cannot leak out less than or equal to the maximum adsorbing capability when the ambient temperature of PCMs exceeds their PTT. Therefore, phase state occurred in a limited and specific area.

The porous materials such as diatomite were widely studied as the supporting materials of form-stable composite PCMs [18–20]. This is because that diatomite has the rich source and such properties as light mass, high porosity, high absorption capability, rigidity and inertness [21, 22]. Based on this, the various fatty acid/diatomite composite PCMs have been prepared by vacuum impregnation and direct impregnation method with different PTT. However, no studies have been carried out to develop the stearic acid/diatomite composites as form-stable PCMs by direct impregnation method to retain thermal inertia in the range of 48–55 °C.

In this study, the stearic acid/diatomite mixtures were prepared as the form-stable composite PCMs using direct impregnation method. The prepared composite PCMs were characterized in terms of chemical compatibility and morphology using Fourier transform infrared (FTIR) spectrometry and X-ray diffraction (XRD) as well as scanning electron microscope (SEM) analysis, respectively. The thermal properties and thermal stability were investigated by differential scanning calorimetry (DSC) and thermogravimetric analysis (TG).

Experimental

Materials

Stearic acid (SA, 99.0 % pure) was supplied by Chengdu Kelong Chemical Reagent Company (Chengdu, China). Diatomite was obtained from China's Pharmaceutical

Industry Co., Ltd (Beijing, China). The chemical composition was shown in Table 1. The diatomite samples were dried in oven at 80 °C for 8 h prior to use.

Preparation of the SA/diatomite composite form-stable PCMs

The SA/diatomite composite PCMs were fabricated by using melt impregnation without vacuum. The treated diatomite was put into six 15-mL beakers with 2 g for each beaker and then SA of different mass was loaded in every beaker, respectively. A series of mass ratio of SA and diatomite was set as 0.2, 0.3, 0.4, 0.5, 0.6, 0.7. After mixing adequately, the beakers were sealed with plastic wrap and placed in oven at 80 °C for 16 h, resulting in the saturated absorption in thermodynamics. During the absorption duration, the sample in every beaker was fully stirred using glass rod every 4 h. Finally, the samples were cooled down to room temperature, and the morphologies of SA/diatomite were observed and recorded in detail.

Characterization

The chemical composition of diatomite sample was analyzed by SEM with energy-dispersive spectrum (EDS) accessory (JSM-7500 F, Japan). The particle size and distribution of diatomite were characterized by Mastersizer 2000 (Malvern Instruments Ltd, England) at 25 °C with the testing range from 0.02 to 2000 μm. Prior to testing, the diatomite powder was treated with ultrasound for 5 min. The structures and compatibility of SA, diatomite and SA/diatomite composite were studied using a Nicolet-560 FTIR spectrometer (USA) with a resolution setting of 4 cm⁻¹ and the scanning range from 4000 to 400 cm⁻¹. The crystalline structures of diatomite, SA and SA/diatomite composite were investigated using the X-ray diffraction (XRD, X'Pert pro MPD, The Netherlands). The melting temperature, freezing temperature and latent heat of SA and SA/diatomite composite were measured by a differential scanning calorimeter (DSC 204 F1, German) at 10 °C min⁻¹ under nitrogen atmosphere. Thermogravimetric analysis (TG) was conducted in a TA Instrument SDT-Q600 thermal analyzer (USA) from 25 to 600 °C under a nitrogen atmosphere. The heating rate was 10 °C min⁻¹ and each sample was about 10 mg for testing. The obtained TG results were analyzed by a TA universal analysis program. The SEM was employed to observe the

Table 1 Chemical composition of the pure diatomite/%

Series	MgO	Al ₂ O ₃	SiO ₂	K ₂ O	CaO	Fe ₂ O ₃	TiO ₂
Diatomite	6.93	12.36	69.84	3.43	2.80	4.21	0.43

surface morphology of diatomite and SA/diatomite composite by a JEOL JSM-5900LV SEM (Japan) with an accelerated voltage of 20 kV. The SEM samples were gold-sputtered before testing.

Results and discussion

Properties of diatomite as the supporting material

In order to better prepare the composite form-stable PCMs, it is very necessary to investigate the properties of diatomite as the supporting material. The EDS graph of diatomite is shown in Fig. 1. As seen from Fig. 1, the element composition of diatomite is Mg, Al, Si, K, Ca, Fe, Ti and O. Among these elements, silicon and oxygen are the two of the most abundant elements with the total amount as high as 81.23 mass%, and others are metallic element, implying that diatomite is composed of silicate, silica or metal oxide. The chemical composition in oxide of diatomite is given in Table 1. The first content of silica reaches 69.84 mass% and the second content of aluminum oxide is up to 12.36 mass%. Metal oxide, silica or silicate has good thermal stability, laying a foundation as the supporting material of composite form-stable PCM, which will be discussed later.

Given the effect on adsorption capability, it is essential to study the particle size and distribution of diatomite before the SA/diatomite composite form-stable PCMs. Figure 2 shows the particle size and distribution of diatomite. As seen from Fig. 2, the curve is trimodal, and the peak particle sizes are corresponding to 0.58, 34.15 and

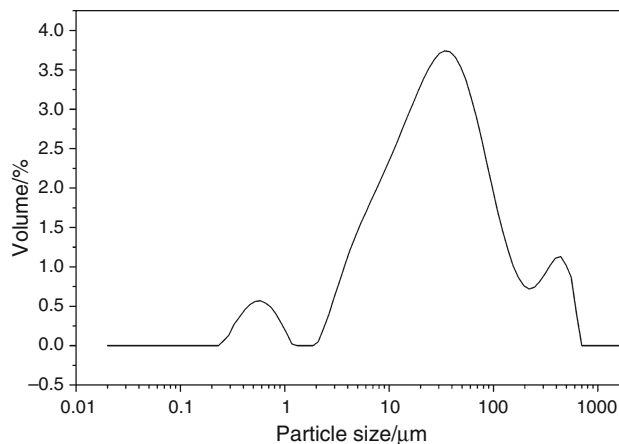


Fig. 2 Particle size and distribution of diatomite

441.02 μm . It is obvious that the integral area of each peak is very unequal, shown in Fig. 2, which represents the relative content of corresponding particles. The particles of 34.15 μm dominate in the whole range. However, the parameter $D[50]$ is representative of the diatomite, as listed in Table 2. Table 2 shows the detailed data of diatomite particle size. The $D[50]$ is only 30.85 μm and the specific surface on mass basis has reached $0.836 \text{ m}^2 \text{ g}^{-1}$, which will facilitate the adsorption of melting SA into the pores of diatomite.

From what is discussed above, the diatomite has good thermal stability and high specific surface area, which is suitable to be used as a supporting material of composite form-stable PCM.

Fig. 1 Energy-dispersive spectroscopy graph of diatomite

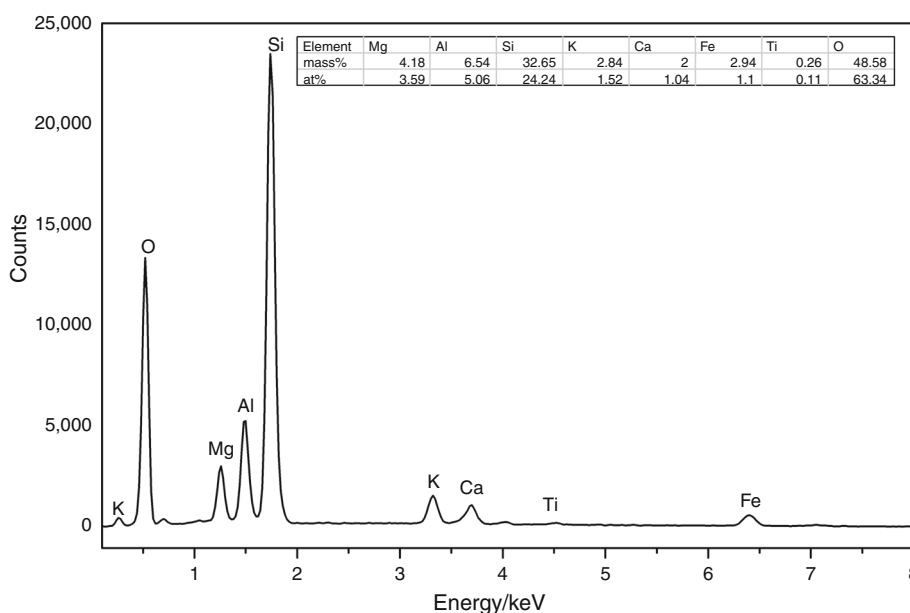


Table 2 Size parameter of diatomite

Sample	$D[10]/\mu\text{m}$	$D[50]/\mu\text{m}$	$D[90]/\mu\text{m}$	$D[3, 4]$	$D[2, 3]$	$\text{SS}/\text{m}^2 \text{g}^{-1}$
Diatomite	5.10	30.85	182.05	72.78	7.17	0.836

The $D[10]$, $D[50]$ and $D[90]$ represented the average particle diameter, when the cumulative percentages were up to 10, 50 and 90 %, respectively. $D[3, 4]$ and $D[2, 3]$ were the volume-average particle diameter and surface area average particle diameter measured by Malvern. SS was specific surface on mass basis

Preparation and microstructure of SA/diatomite form-stable PCMs

SA/diatomite composite form-stable PCMs were prepared using a direct impregnation method without vacuum, which was considered as a facile and robust strategy for paving materials. To maximize the adsorption capacity, a series of mass ratio (MR) of SA and diatomite were designed with the MR changing from 0.2 to 0.7 in step size of 0.1. The diatomite still maintains granular when the MR of SA and diatomite is 0.2, 0.3, 0.4. However, the diatomite powders obviously become into a block when the MR of SA and diatomite arrives at 0.4, revealing that the loaded SA probably surpasses the adsorption capacity of diatomite in a specific condition. Therefore, the SA/diatomite composite form-stable PCM was put on a dried filter paper at 80 °C to remove the adsorption of SA on the surface of diatomite, avoiding the possible leakage in potential paving application.

Figure 3 shows the SEM images of diatomite and SA/diatomite composite form-stable PCM. In Fig. 3a, many tunnel-like veins are detected on the surface of diatomite, indicating the surface inhomogeneity. The uneven surface of diatomite is ascribed to the pores where the SA would be absorbed by capillary and surface tension force [23]. In Fig. 3b, the surface of SA/diatomite composite has become smooth, resulting from the SA has been fixed in the pores of diatomite. The protuberant edge also gradually gets even and glossy. By comparison, the SA/diatomite composite form-stable PCM has been successfully prepared based on the facile direct impregnation method.

Chemical compatibility of SA/diatomite composite form-stable PCM

FTIR spectra of diatomite, SA and SA/diatomite composite are shown in Fig. 4. The characteristic peaks of diatomite in Fig. 4a at 3435, 1638, 1429, 1079 and 789 cm^{-1} are detected. The band at 3435 cm^{-1} is the stretching vibration peak of free silanol groups (SiO–H) in diatomite, and the peak at 1079 cm^{-1} reflects the stretching vibration of siloxane (–Si–O–Si–) group in

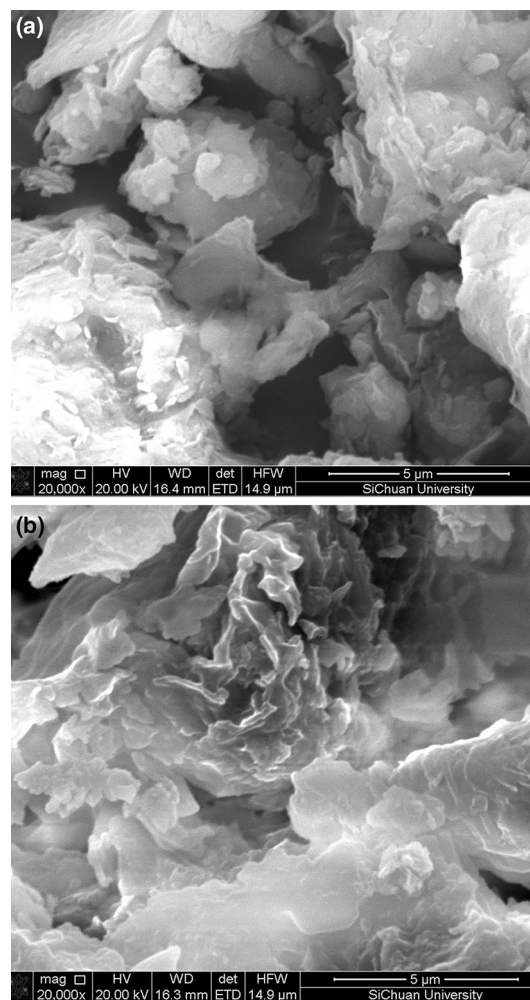


Fig. 3 SEM photographs of **a** diatomite and **b** form-stable SA/diatomite composite PCM

diatomite. The peak at 789 cm^{-1} is ascribed to the bending vibration of SiO–H. In Fig. 4b, the peaks at 2914 and 2859 cm^{-1} are the stretching vibration peaks of –CH₃ and –CH₂– in SA and the peaks at 1700 and 1467 cm^{-1} are the stretching vibration peaks of C=O and C–O groups of SA. As seen from Fig. 4c, the peaks at 3435, 1638, 1429 and 789 cm^{-1} , attributed to the stretching or bending vibration of diatomite groups, are observed, indicating the existence of diatomite in composite PCM. Meanwhile, the peaks at 2914, 2851, 1700 and 1473 cm^{-1} , ascribed to

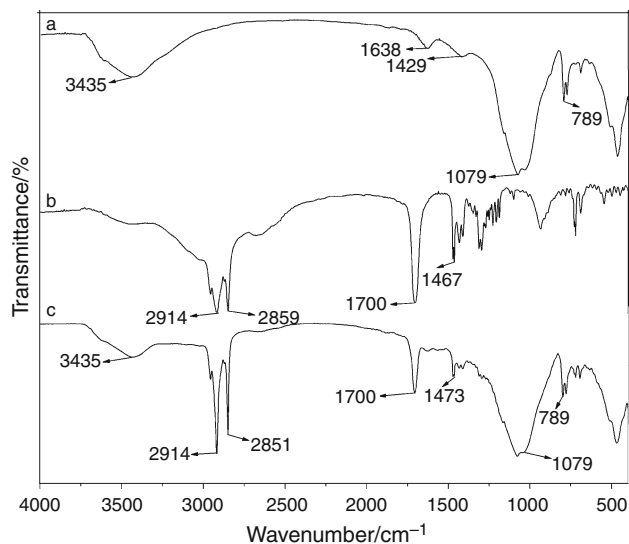


Fig. 4 FTIR spectra of *a* diatomite, *b* SA and *c* form-stable SA/diatomite composite PCM

the stretching vibration of SA groups, are also detected, revealing the existence of SA in composite PCM. No new peaks are observed, indicating that there are only physical interactions between diatomite and SA in composite PCM. The physical interactions mainly contain capillary and surface tension force, preventing the melting SA from leaking out when the ambient temperature exceeds the PTT of SA resulting in the melting of SA.

Figure 5 shows the XRD diffractograms of diatomite, SA and SA/diatomite composite form-stable PCM, and the detailed diffraction peak information is listed in Table 3. As seen from Fig. 5, all samples have obvious diffraction peaks, confirming the existence of crystalline structure. In Fig. 5a, diatomite has strong diffraction at 20.8° and 26.6° , corresponding to the crystal face of (100) and (101), respectively. The intensity of peak at 20.8° is 23.80 % based on that at 26.6° . Obtained from Bragg's law, the interplanar spacing is 4.24 and 3.34 Å, respectively. In Fig. 5b, SA shows sharp peaks at 21.5° and 23.9° due to its regular crystal. The relative intensity of peak at 23.9° is 61.03 % with respect to that at 21.5° . In Fig. 5c, the peaks at 20.8° , 21.5° , 23.9° and 26.6° are observed, indicating the existence of SA and diatomite in composite form-stable PCM and simple physical interactions between SA and diatomite. As shown in Table 3, the relative intensity of peaks at 20.8° , 21.5° , 23.9° and 26.6° is 21.25, 38.81, 9.12 and 100 %, respectively, based on the intensity of peak at 26.6° . Comparing the intensities of 20.8° and 26.6° peaks, the relative intensity is almost unchanged, indicating that the crystalline structure is not affected in the preparation process of SA/diatomite composite due to that the preparation temperature of composite form-stable PCM is far lower than the melting

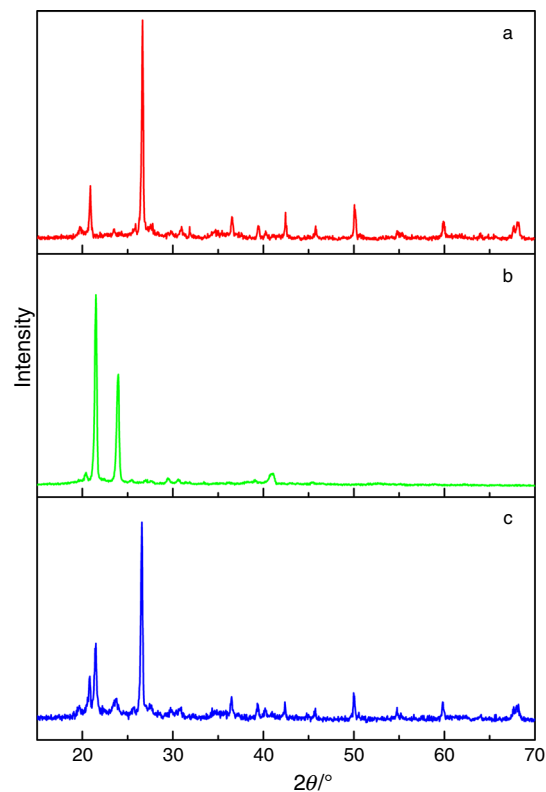


Fig. 5 XRD diffractograms of *a* diatomite, *b* SA and *c* form-stable SA/diatomite composite PCM

point of diatomite. However, the relative intensity of peak at 23.9° in Fig. 5c is 23.49 % with respect to that at 21.5° , lower than 61.03 % of the counterpart in Fig. 5b. The change of relative intensity at 21.5° and 23.9° indicates the decrease in big crystalline grains and increase in small crystalline grains due to the limitation of pores in diatomite. By comparison with Fig. 5b, c, the absolute intensity at 21.5° and 23.9° decreases, ascribed to the lower mass percentage of SA in SA/diatomite composites. But no new diffraction peaks have been observed in Fig. 5c, revealing that the crystal type is not influenced by the composite technology of SA/diatomite composite form-stable PCM with the decrease in crystal size and that only physical interactions exist in SA/diatomite composite after the direct impregnation treatment.

Thermal properties of SA/diatomite composite form-stable PCMs

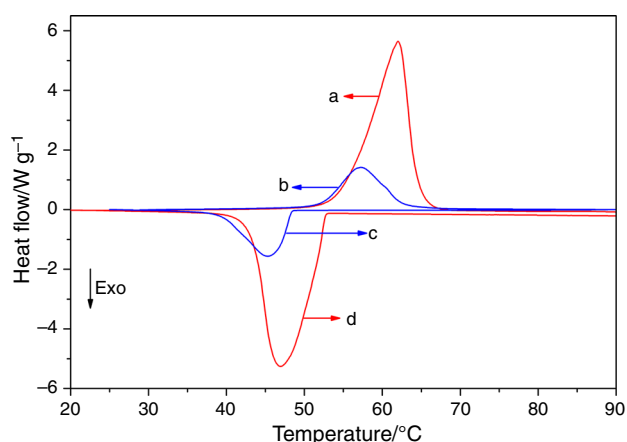
DSC analysis is carried out to investigate the PTT and latent heat of SA and SA/diatomite composite as significant parameters of PCMs, and Fig. 6 shows the typical DSC curves of SA and SA/diatomite composite. As seen from Fig. 6a, d, the respective melting and freezing temperatures are 55.1 and 52.8 °C with a supercooling degree of 2.3 °C in accord with prior reports [24–26]. Figure 6b, c shows

Table 3 XRD data of diatomite, SA and SA/diatomite composite

Sample	$2\theta/^\circ$	Interplanar spacing/ \AA	Relative intensity/%
Diatomite	20.89	4.24	23.80
	26.65	3.34	100
SA	21.52	4.12	100
	23.96	3.71	61.03
SA/diatomite composite form-stable PCM	20.89	4.24	21.25
	21.52	4.12	38.81
	23.96	3.71	9.12
	26.65	3.34	100

52.3 °C of melting temperature and 48.4 °C of freezing temperature of SA in SA/diatomite composite with a supercooling degree of 3.9 °C, possibly due to the reduction in crystal nucleus [27]. The supercooling degree of SA/diatomite composite is higher than that of pristine SA, indicating that the diatomite has a negative effect on the crystallization of SA. However, the supercooling degree of SA/diatomite composite is still low. Different from the sharp peaks of SA in Fig. 6a, d, the blunt melting and freezing peaks in Fig. 6b, c appear because of the different degree of crystallization structure, confirming that the pore size has a effect on crystal size mentioned above.

The melting and freezing temperatures and latent heat obtained from the DSC curves are given in Table 4. The melting and freezing latent heat are 197.9 and 195.5 J g⁻¹ for SA and 57.1 and 57.1 J g⁻¹ for SA/diatomite composite (S0.4), respectively. The melting and freezing latent heat of SA/diatomite composite are almost same as each other, indicating that the composite form-stable PCM has good thermal repetition and that the crystallinity of SA is not affected by diatomite when the crystal size decreases. To further determine the maximum adsorption of SA in diatomite, the PTT and latent heat of SA/diatomite composite

**Fig. 6** DSC curves of a, d SA and b, c form-stable SA/diatomite composite PCM

(S0.3) are also exhibited in Table 4. For absolute value of latent heat, the melting and freezing latent heat of (S0.3) are obviously lower than those of (S0.4), meaning that the loaded SA amount of (S0.3) is under the maximum adsorption capacity of diatomite in the specific condition. The mass percentage (MP) of SA in SA/diatomite composite reaches 29 mass% based on latent heat of (S0.4) and 28.5 mass% by gravimetry, which is calculated from Eqs. (1) and (2).

$$MP = (\Delta H_c / \Delta H_0) \times 100 \% \quad (1)$$

$$MP = [MR / (MR + 1)] \times 100 \% \quad (2)$$

where MP is the mass percentage of SA in SA/diatomite composite form-stable PCM; ΔH_c is the latent heat of SA/diatomite composite form-stable PCM, J g⁻¹; ΔH_0 is the latent heat of pure SA, J g⁻¹.

Based on the above discussion, diatomite has slight effect on the PTT of SA, meaning that the form-stable method by absorbing the SA in diatomite has no influence on application of the SA at a certain temperature range. Given the proper PTT and much latent heat, the SA/diatomite composite has potential as paving materials for application, retaining the thermal inertia around 50 °C to avoid the damage of pavement induced by big temperature difference. The SA/diatomite composite can absorb lots of heat from the surrounding during hot day and release amounts of heat at cold night.

Thermal energy storage characteristics of different form-stable composite PCMs in literature [28–33] are listed in Table 5. It can be seen that the latent heat of SA/diatomite composite form-stable PCM in present study is higher than some organic–inorganic hybrid composite form-stable PCMs available in literature.

Thermal stability of SA/diatomite composite form-stable PCM

For composite form-stable PCM, a high thermal stability is significant and essential [34, 35]. The thermal

Table 4 Latent heat storage properties of SA and the SA/diatomite composite with the various LA content

PCM	Melting point/°C	Latent heat of melting/J g ⁻¹	Freezing point/°C	Latent heat of freezing/J g ⁻¹
SA	55.1	197.9	52.8	-195.5
SA/diatomite composite (S0.4) ^a	52.3	57.1	48.4	-57.1
SA/diatomite composite (S0.3) ^b	52.0	52.2	48.3	-51.5

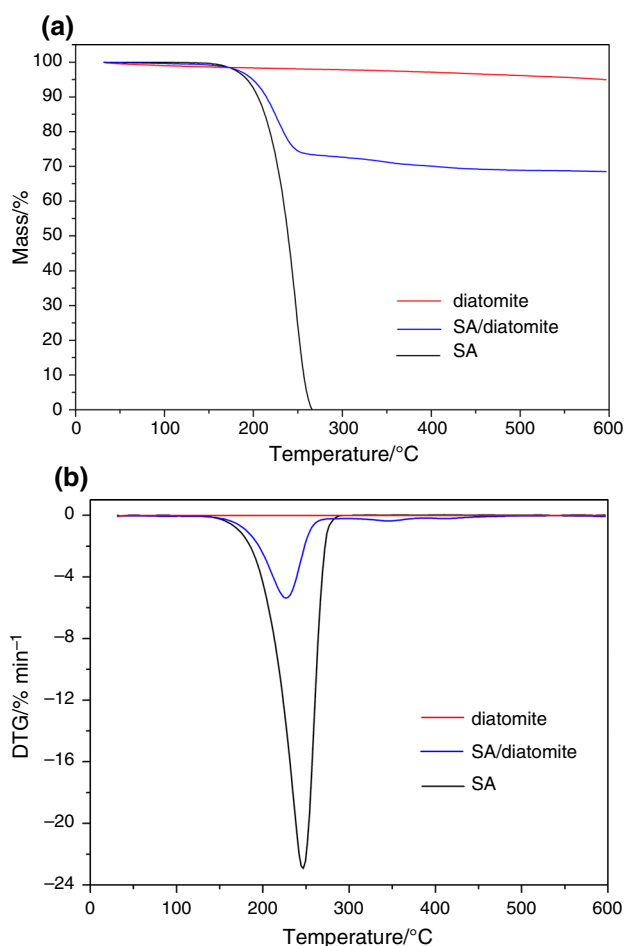
^a The mass ratio of SA and diatomite is 0.4 (i.e., 2 g of diatomite and 0.8 g of SA)

^b The mass ratio of SA and diatomite is 0.3 (i.e., 2 g of diatomite and 0.6 g of SA)

Table 5 Thermal energy storage characteristics of different form-stable composite PCMs in literature

Composite PCM	Melting point/°C	Freezing point/°C	Latent heat/J g ⁻¹	References
Capric–myristic acid/VMT/2 mass%EG	19.7	17.1	26.9	[28]
Paraffin/bentonite	41.7	43.4	39.84	[29]
RT20/montmorillonite	20.8	–	53.6	[30]
Capric acid/halloysite nanotube	28.64	25.08	56.85	[31]
Capric–myristic acid (20 mass%)/vermiculite	23.35	14.54	27.46	[32]
Lauric–stearic acid (38 mass%)/gypsum	34.0	–	50.3	[33]
Stearic acid/diatomite (S0.4)	52.3	48.4	57.1	Present study

stability of SA/diatomite composite was evaluated by TG analysis. Figure 7 shows the TG and DTG curves of diatomite, SA and SA/diatomite composite. As seen from Fig. 7a, the mass loss of diatomite is less than 5 mass% when the testing temperature changes from 25 to 600 °C, which is caused by impurities. In Fig. 7a, b, only a decomposition stage exists for pristine SA. The decomposition of SA starts at 207 °C and ends at 262 °C, when the maximum decomposition rate of SA from Fig. 7b occurs at 246 °C. It can be seen in Fig. 7a, b that the first decomposition stage of SA/diatomite composite starts at 192 °C and ends 246 °C, ascribed to degradation of SA in SA/diatomite composite. In Fig. 7b, the SA/diatomite composite decomposes faster when the temperature reaches 226 °C. The mass of SA/diatomite composite further decreases when the temperature changes from 246 to 600 °C due to the existence of impurities mentioned above. By comparison, the initial and maximum decomposition temperatures of SA/diatomite composite are, respectively, 15 and 20 °C lower than that of pristine SA, indicating that the interaction between SA and diatomite reduces the thermal stability of SA. However, the initial decomposition temperature of SA/diatomite composite still reaches up to 192 °C. Moreover, the TG curves confirm that the impregnation ratio of SA in SA/diatomite composite form-stable PCM reaches 30 mass%, consistent with that obtained from DSC measurement. Derived from TG analysis, the SA/diatomite composite form-stable PCM has a good thermal stability.

**Fig. 7** TG (a) and DTG (b) curves of diatomite, SA and form-stable SA/diatomite composite PCM

Conclusions

SA/diatomite composite form-stable PCM has been prepared by using a direct impregnation method without vacuum. FTIR and XRD results indicate that there are only physical interactions between SA and diatomite in SA/diatomite composite form-stable PCM. Meanwhile, XRD analysis confirms that the crystal type is not affected by composite technology of SA/diatomite composite form-stable PCM and the crystal size of SA in SA/diatomite composite decreases due to the limited pores in diatomite. The melting and freezing temperatures are 52.3 and 48.4 °C, respectively. The latent heat of SA/diatomite composite form-stable PCM reaches 57.1 J g⁻¹, enough to be used in a practical application. TG result reveals that the SA/diatomite composite form-stable PCM has a good thermal stability with the decomposition temperature of up to 200 °C. The prepared SA/diatomite composite form-stable PCM has a great potential as paving materials for application.

References

- Sanchez L, Sanchez P, Lucas A. Microencapsulation of PCMs with a polystyrene shell. *Colloid Polym Sci.* 2007;285:1377–85.
- Li W, Song G, Tang G, Chu X, Ma S, Liu C. Morphology, structure and thermal stability of microencapsulated phase change material with copolymer shell. *Energy.* 2010;36:785–91.
- Giro-Paloma J, Konu klu Y, Fernandez A. Preparation and exhaustive characterization of paraffin or palmitic acid microcapsules as novel phase change material. *Sol Energy.* 2015;112:300–9.
- He F, Wang X, Wu D. Phase-change characteristics and thermal performance of form-stable n-alkanes/silica composite phase change materials fabricated by sodium silicate precursor. *Renew Energy.* 2015;74:689–98.
- Yang X, Yuan Y, Zhang N, Cao X, Liu C. Preparation and properties of myristic–palmitic–stearic acid/expanded graphite composites as phase change materials for energy storage. *Sol Energy.* 2014;99:259–66.
- Fang X, Fan L, Ding Q, Yao X, Wu Y, Hou J, Wang X, Yu Z, Chneg G, Hu Y. Thermal energy storage performance of paraffin-based composite phase change materials filled with hexagonal boron nitride nanosheets. *Energy Convers Manag.* 2014;80:103–9.
- Zhang Z, Fang X. Study on paraffin/expanded graphite composite phase change thermal energy storage material. *Energy Convers Manag.* 2006;47:303–10.
- Sari A, Karaipekli A. Thermal conductivity and latent heat thermal energy storage characteristics of paraffin/expanded graphite composite as phase change material. *Appl Therm Eng.* 2007;27:1271–7.
- Wang L, Meng D. Fatty acid eutectic/polymethyl methacrylate composite as form-stable phase change material for thermal energy storage. *Appl Energy.* 2010;87:2660–5.
- Tyagi V, Kaushik S, Tyagi S, Akiyama T. Development of phase change materials based microencapsulated technology for buildings: a review. *Renew Sustain Energy Rev.* 2011;15:1373–91.
- Sun Z, Zhang Y, Zheng S, Park Y, Frost R. Preparation and thermal energy storage properties of paraffin/calcined diatomite composites as form-stable phase change materials. *Thermochim Acta.* 2013;558:16–21.
- Sanchez L, Sanchez P, Lucas A. Microencapsulation of PCMs with a polystyrene shell. *Colloid Polym Sci.* 2007;285:1377–85.
- Song Q, Li Y, Xing J, Hu J, Marcus Y. Thermal stability of composite phase change material microcapsules incorporated with silver nano-particles. *Polymer.* 2007;48:3317–23.
- Xu B, Li Z. Paraffin/diatomite composite phase change material incorporated cement-based composite for thermal energy storage. *Appl Energy.* 2013;105:229–37.
- Yang X, Yuan Y, Zhang N, Cao X, Liu C. Preparation and properties of myristic–palmitic–stearic acid/expanded graphite composites as phase change materials for energy storage. *Sol Energy.* 2014;99:259–66.
- Xu B, Li Z. Paraffin/diatomite/multi-wall carbon nanotubes composite phase change material tailor-made for thermal energy storage cement-based composites. *Energy.* 2014;72:371–80.
- Li M, Wu Z, Kao H. Study on preparation and thermal properties of binary fatty acid/diatomite shape-stabilized phase change materials. *Sol Energy Mater Sol Cells.* 2011;95:2412–6.
- Li M, Kao H, Wu Z, Tao J. Study on preparation and thermal property of binary fatty acid and the binary fatty acids/diatomite composite phase change materials. *Appl Energy.* 2011;88:1606–12.
- Li M, Wu Z, Kao H. Study on preparation, structure and thermal energy storage property of capric–palmitic acid/attapulgit composite phase change materials. *Appl Energy.* 2011;88:3125–32.
- Sari A, Bicer A. Thermal energy storage properties and thermal reliability of some fatty acid esters/building material composites as novel form-stable PCMs. *Sol Energy Mater Sol Cells.* 2012;101:114–22.
- Karaman S, Karaipekli A, Sari A, Bicer A. Polyethylene glycol (PEG)/diatomite composite as a novel form-stable phase change material for thermal energy storage. *Sol Energy Mater Sol Cells.* 2011;95:1647–53.
- Fu X, Liu Z, Xiao Y, Wang J, Lei J. Preparation and properties of lauric acid/diatomite composites as novel form-stable phase change materials for thermal energy storage. *Energy Build.* 2015;104:244–9.
- Xu B, Li Z. Paraffin/diatomite composite phase change material incorporated cement-based composite for thermal energy storage. *Appl Energy.* 2013;105:229–37.
- Sari A, Alkan C, Altintas A. Preparation, characterization and latent heat thermal energy storage properties of micro-nanoencapsulated fatty acids by polystyrene shell. *Appl Therm Energy.* 2014;73:1160–8.
- Yuan Y, Zhang N, Tao W, Cao X, He Y. Fatty acids as phase change materials: a review. *Renew. Renew Sustain Energy Rev.* 2014;29:482–98.
- Zhou D, Zhao C, Tian Y. Review on thermal energy storage with phase change materials (PCMs) in building applications. *Appl Energy.* 2012;92:593–605.
- Zhang X, Fan Y, Tao X, Yick K. Crystallization and prevention of supercooling of microencapsulated n-alkanes. *J Colloid Interface Sci.* 2005;281:299–306.
- Karaipekli A, Sari A. Capric–myristic acid/vermiculite composite as form-stable phase change material for thermal energy storage. *Sol Energy.* 2009;83:323–32.
- Li M, Wu Z, Kao H, Tan J. Experimental investigation of preparation and thermal performances of paraffin/bentonite composite phase change material. *Energy Convers Manag.* 2011;52:3275–81.
- Zhou X, Xiao H, Feng J. Preparation and thermal properties of paraffin/porous silica ceramic composite. *Colloid Polym Sci.* 2009;69:1246–9.
- Mei D, Zhang B, Liu R, Zhang Y, Liu J. Preparation of capric acid/halloysite nanotube composite as form-stable phase change material for thermal energy storage. *Sol Energy Mater Sol Cells.* 2011;95:2772–7.

32. Karaipekli A, Sari A. Capric–myristic acid/vermiculite composite as form-stable phase change material for latent heat thermal energy storage. *Renew Energy*. 2008;33:2599–605.
33. Rozanna D, Salmiah A, Chuah T, Medyan R, Thomas Choog SY, Saari M. A study on thermal characteristics of phase change material (PCM) in gypsum board for building application. *J Oil Palm Res*. 2005;17:41–6.
34. Fu X, Kong W, Zhang Y, Jiang L, Wang J, Lei J. Novel solid–solid phase change materials with biodegradable trihydroxy surfactants for thermal energy storage. *RSC Adv*. 2015;5:68881–9.
35. Genc ZK, Canbay CA, Acar SS, Sekerci M, Genc M. Preparation and thermal properties of heterogeneous composite phase change materials based on camphene–palmitic acid. *J Therm Anal Calorim*. 2015;120:1679–88.